

Determining the Isotopic Composition of Surface Water Vapor Flux From High-Frequency Observations Using Flux-Gradient and Keeling Plot Methods

Yongbo Hu¹, Wei Xiao¹, Zhongwang Wei^{3, 4}, Lisa R. Welp⁵, Xuefa Wen⁶, Xuhui Lee²

¹Yale-NUIST Center on Atmospheric Environment, International Joint Laboratory on Climate and Environment Change (ILCEC), Nanjing University of Information Science and Technology, Nanjing, China.

²School of Forestry and Environmental Studies, Yale University, New Haven, Connecticut, USA.

³Guangdong Province Key Laboratory for Climate Change and Natural Disaster Studies, School of Atmospheric Sciences, Sun Yat-sen University, Guangzhou, China

⁴Southern Marine Science and Engineering Guangdong Laboratory (Zhuhai), Zhuhai, China

⁵Department of Earth, Atmospheric, and Planetary Sciences, Purdue University, West Lafayette, Indiana, USA

⁶Institute of Geographic Sciences and Natural Resources Research, Chinese Academy of Sciences, Beijing, China.

Corresponding author: Xuhui Lee (xuhui.lee@yale.edu); Wei Xiao (xiaowei_522@163.com)

Key Points:

- Compared with factory-specified errors, field characterization of errors of IRIS instruments can improve parameter estimation of the York's solution regression
- Good agreement is achieved among the flux-gradient, the Keeling plot method using York's solution, and the Keeling plot method using ordinary least squares
- The Keeling plot method gives better results by using measurements made at two heights than at only one height

- 24 • Ordinary least squares is the least biased regression model against the Craig-Gordon
25 prediction

Abstract

The isotopic composition of surface water vapor flux (δ_E) is a quantity frequently used to investigate the local and regional water cycle. This study reports the results of a comparative evaluation of δ_E determined with the Keeling plot and the flux-gradient methods using high-frequency data collected at a cropland site and a lake site. Three regression models, ordinary least squares (OLS), York's solution (YS), and geometric mean regression (GMR), were tested with the Keeling plot method. Results show that field characterization of measurement errors can improve the estimation of the YS regression. For both sites, broad agreement was achieved between the Keeling plot method with YS regression, the Keeling plot method with OLS regression and the flux-gradient method. For the lake site, OLS was the least biased of the three regression models in reference to the δ_E calculated by the Craig-Gordon model of isotopic evaporation of open water. These results favor the OLS over the YS regression for studies of isotopic evaporation when measurement errors in field conditions are unavailable.

1 Introduction

The isotopic composition of surface water vapor flux (δ_E) is a key parameter in studies of the water cycle using isotopic tracer methods. It is used for estimating lake evaporation (Gibson et al., 1993; Xiao et al., 2017), constraining local moisture recycling (Bowen et al., 2019; Gat et al., 1994; Griffis et al., 2016; Wang et al., 2016; Xiao et al., 2018), characterizing sources of moisture in the atmospheric boundary layer (Lee et al., 2007; Simonin et al., 2014; Welp et al., 2008, 2012; Zannoni et al., 2019a), and partitioning of evapotranspiration in ecosystems (Good et al., 2014, 2015; Lu et al., 2017; Sun et al., 2019; Wei et al., 2018; Wen et al., 2016). The Keeling plot method and the flux-gradient method are two common measurement strategies for determining δ_E . Each strategy requires certain conditions about atmospheric mixing near the ground. The Keeling plot method was originally developed for CO_2 . By extending it to water vapor, it assumes (i) that surface evaporation is solely responsible for observed variations in the isotopic composition of water vapor δ_v and in the water vapor concentration c , and (ii) that δ_E remains invariant during the observational period. The mixing of the evaporated vapor with vapor in the surface-layer air can be described by (Wang & Yakir, 2000; Yepez et al., 2003)

$$\delta_v = a + b(1/c) \quad (1)$$

where a and b are intercept and slope coefficients, respectively. If the two underlying assumptions are satisfied, the intercept coefficient a is equivalent to δ_E . Typically, Eq. (1) is applied to time series of δ_v and c measured at a single height with a regression procedure to obtain an estimate of a .

Before isotope ratio infrared spectroscopy (IRIS) instruments became available, application of the Keeling plot method involved measurement of water vapor concentration, c ,

and collection of water vapor via cold traps for determination of δ_v . In order to obtain enough trapped samples for the regression analysis, the observation period often extended several hours or longer (Delattre et al., 2015; Yepez et al., 2003, 2005; Zannoni et al., 2019b). However, temporal changes in atmospheric forcing, such as relative humidity and cloudiness, can cause large short-term (minutes to hours) fluctuations in δ_E of land evapotranspiration (Dubbett & Werner, 2019; Good et al., 2012; Lee et al., 2007; Quade et al., 2019; Welp et al., 2008; Wen et al., 2016) and open-water evaporation (Xiao et al., 2017). One consequence of δ_E variations is that δ_v may no longer be linear with $1/c$. When this occurs, the validity of the second Keeling plot assumption, that δ_E remains invariant during the observational period, is questionable (Pataki et al., 2003). Furthermore, if the observation period is too long, temporal changes in δ_v and c can result from mesoscale and synoptic-scale atmospheric events unrelated to surface evaporation, even at a measurement height very close to the surface, raising doubt about the first Keeling plot assumption, that surface evaporation is solely responsible for observed variations (Lee et al., 2006). Obviously, when one or both of the Keeling plot method assumptions are violated, the intercept coefficient a is no longer a true representation of δ_E , regardless of which regression model is used for parameter estimation.

The flux-gradient method determines δ_E from the ratio of the vertical concentration gradient of the minor to that of the major isotopologue (e.g., Lee et al., 2007). The molar ratio of the H_2^{18}O flux to the H_2^{16}O flux is given by

$$R_E = (c_2^i - c_1^i)/(c_2 - c_1) \quad (2)$$

where c^i and c denote the mean molar mixing ratio of H_2^{18}O and H_2^{16}O of an observation period, respectively, and subscripts 1 and 2 denote the upper and the lower measurement level,

respectively. The molar flux ratio R_E is then converted to the δ scale to give δ_E . Because the flux-gradient method uses high frequency data over a short period (typically one hour), this method can capture temporal changes in δ_E . Calculation of δ_E with Eq. (2) is mathematically unambiguous if the mixing ratios are measured with an IRIS instrument. Occasionally a hybrid measurement technique is used: the $H_2^{16}O$ mixing ratio is measured with an in-situ instrument and δ_v is determined with mass-spectrometer analysis of the vapor samples collected with cold traps (Yakir & Wang, 1996). In this case, Eq. (2) can be rearranged to give δ_E (Good et al., 2002). The flux-gradient method assumes that the diffusion of the $H_2^{18}O$ and $H_2^{16}O$ molecules is identically efficient in the atmospheric surface layer so that the diffusivity coefficient cancels out when performing the flux ratio calculation (Griffis et al., 2005). Another implicit assumption is that the footprint of measurement at the upper level and that at the lower level lie in the same source area (Griffis et al., 2007). In situations where the two measurement heights are far apart vertically or where the fetch of the target surface is limited, the evaporation of a source upwind of the target surface can “contaminate” the upper measurement more than the lower measurement, causing errors in the measured flux and the flux ratio (Horst, 1999).

While determination of δ_E with the flux-gradient method is mathematically unambiguous, the Keeling plot result depends on the choice of statistical regression model. Because the intercept of Eq. (1) is obtained by extrapolation far beyond the observed data range, the result is very sensitive to how the regression parameters are obtained. A large body of papers have been published on this topic regarding the isotopic composition of terrestrial CO_2 flux (e. g., Chen et al., 2017; Kayler et al., 2010; Ogée et al., 2003; Pataki et al., 2003; Wehr & Saleska, 2017; Zobitz et al., 2006). The ordinary least squares (OLS) regression model, the most common model

for estimating the regression coefficients, assumes that all measurement errors occur in the dependent variable (δ_v , Eq. (1)) and no errors exist in the independent variable (concentration, c). However, the concentration data can also suffer from measurement errors. For this reason, some researchers recommend that the geometric mean regression (GMR) model or orthogonal distance regression (ODR) model should be used (Ogée et al., 2003; Pataki et al., 2003). Zobitz et al. (2006) applied the OLS and the GMR method to the CO_2 isotope and concentration time series obtained with both isotope ratio mass spectroscopy (IRMS) and IRIS instruments, and found that the difference between the two regression methods is caused by biases in the GMR regression. Chen et al. (2017) also showed that the OLS performs better than the GMR for an IRIS instrument. More recently, Wehr and Saleska (2017) used a general regression model, named here the York's solution (YS) model and recommended the YS model to be used in the Keeling plot method. Their recommendation is based on the fact that YS takes into account error structures of the independent and dependent variables separately and also the correlation between these two types of error.

The error structures are important input parameters for accurate fitting of the regression line. In Wehr and Saleska's evaluation of the YS model, errors in the dependent and independent variables are prescribed with hourly concentration-independent instrument precisions specified by the manufacturer for controlled conditions, and error correlation between the two variables is omitted. However, the precision of δ_v changes with the water vapor concentration (Salmon et al., 2019; Sturm & Knohl, 2010). Therefore, it may be possible to further improve the YS model by using errors and error correlation characterized in field conditions.

With the IRIS technology, it is possible to apply the Keeling plot method to the high-frequency c and δ_v time series data collected in short observation periods (e.g., 1 h). The idea of applying the Keeling plot method to high frequency time series was first proposed by Bowling et al. (1999) before the emergence of the IRIS technology and was later tested with CO₂ isotope data collected with an IRIS instrument (Griffis et al., 2004). Because the data are collected at a high frequency, the sample size is large (typically > 700 in one hour), effectively increasing the variability in the observed water vapor concentration and decreasing the uncertainty of parameter estimation (Good et al., 2012). By restricting the regression to a short period (hourly), errors arising from the two underlying assumptions should be small. Therefore, it is possible to determine δ_E using the same data with either the Keeling plot method or the flux-gradient method. A practical question is whether these two methods agree with each other under field conditions.

Another practical issue concerns bias errors of the Keeling plot and the flux-gradient methods due to non-ideal experimental conditions. As mentioned earlier, in the case of the Keeling plot method, bias errors can occur even with a perfect statistical model, if the underlying assumptions about atmospheric mixing are not met. Assessment of systematic biases is challenging for land ecosystems because the true δ_E is not known *a priori*, even in isotopic steady state. In isotopic steady state, the isotopic composition of plant transpiration approaches that of the xylem water which is a measurable quantity, but δ_E of evapotranspiration is also influenced by soil evaporation whose isotopic composition is generally unknown (Yakir & Sternberg, 2000). To overcome a similar problem for CO₂, some researchers used synthetic data that combines a hypothetical flux isotopic signal with random variations superimposed on the

concentration and the δ variable (Chen et al., 2017; Kayler et al., 2010; Vardag et al., 2016; Wehr & Saleska, 2017; Zobitz et al., 2006). This synthetic approach is less feasible for water vapor because it is difficult to assign a representative value for δ_E due to its high temporal variability. According to in-situ observations of Welp et al. (2008), δ_E can vary by as much as 40‰ in the course of a day.

In this study, we tested a new strategy to assess bias errors, using data collected at a lake site. Here, the benchmark is the δ_E calculated with the Craig-Gordon model of the isotopic composition of open-water evaporation (Craig & Gordon, 1965). Inputs required by the model include measurements of δ_v , air humidity, water surface temperature, and the isotopic composition of the lake water. Because the model is grounded on well-established principles of equilibrium and kinetic fractionation of open-water evaporation (Gonfiantini et al., 2018), it can provide an independent and unbiased estimate of δ_E for evaluating the Keeling plot and the flux-gradient methods.

In this paper, we report the results of a comparative evaluation of the Keeling plot method and the flux-gradient method using high-frequency data collected with IRIS instruments at a cropland site and a lake site. The fetch of the lake site is extensive (> 8 km) and that of the cropland is more limited (about 200 m). Wehr and Saleska (2017) have conducted a comprehensive evaluation of the Keeling plot method for CO_2 . The analysis presented below can be viewed as a test of their findings for water vapor. The specific objectives of this study are (1) to determine if field characterization of error structures of the IRIS instruments can improve parameter estimation of the YS regression, (2) to characterize the relative agreement between the

flux-gradient method and the Keeling plot method with three regression models (OLS, GMR and YS), and (3) to evaluate bias errors of the Keeling plot method and the flux-gradient method against the Craig-Gordon model prediction. Even though hydrogen isotopes were also measured in the two experiments, we restrict our analysis to oxygen isotopes.

2 Materials and Methods

2.1 Sites and instruments

The datasets used in this study were obtained in two field experiments. The first experiment was conducted in an irrigated maize field in Zhangye, Gansu Province, in Northwest China (38° 51' N, 100° 22' E) in 2012 (Wen et al., 2016). The fetch was greater than 200 m. The H₂O, HDO and H₂¹⁸O concentrations were measured at two heights (0.5 m and 1.5 m) above the canopy with an IRIS water vapor isotope analyzer (Model L1102-i, Picarro Inc. CA, USA) at 0.2 Hz. The hourly precision for the vapor $\delta^{18}\text{O}$ is ~0.2‰ (Wen et al., 2012b). The analyzer was customized to improve its time response. Switching between the two intake heights occurred every 2 min and the measurement became stable after 25 s (5 datapoints; Wen et al., 2016, their Figure 1). The last 8 datapoints after each switching, corresponding to the last 40 seconds, were used in the analysis. The analyzer was calibrated in-situ with a liquid vaporization module (Picarro Inc.) and a CTC Analytics Prep and Load liquid autosampler (LEAP Technologies, Carrboro, NC, USA) using a single liquid water standard with a $\delta^{18}\text{O}$ value of -14.29‰. There were 3 concentrations of calibration vapor, each measured for 25 min. After each calibration, three hours were spent on the measurement of ambient air. A linear interpolation between two consecutive calibration cycles was used to obtain the span for correcting the ambient air measurements (Huang & Wen, 2014; Wen et al., 2008, 2012a).

The other experiment was in the northern part of Lake Taihu conducted at Meiliangwan (MLW, 31° 15' N, 120° 13' E) as part of the Taihu Eddy Flux Network (Lee et al., 2014) between August 2012 and September 2016. Lake Taihu is located in the Yangtze River Delta in Eastern China. The H₂O, HDO and H₂¹⁸O concentrations were measured at two heights (1.1 m and 3.5 m) above the water surface with an IRIS water vapor isotope analyzer (Model 911-0004; Los Gatos Research, Mountain View, CA, USA) at 2 Hz. The 2-min precision of this instrument for the vapor $\delta^{18}\text{O}$ is 0.2‰ (Xiao et al., 2017). This analyzer was also modified to allow high sampling flow to improve its time response. Switching between the two intakes occurred every 30 s, and the measurement became stable in 5 s (about 10 datapoints; Xiao et al., 2017, their Figure 3). In this study, the last 15 datapoints, corresponding to the last 7.5 seconds, were used for calculations. The measurement site was located 250 m from the northern shore. To minimize land influence on the measurement, we restricted our analysis to the data collated in the wind direction sector of 140° to 315°, corresponding to a fetch of 8 km to 50 km. The in-situ calibration vapor was generated by a water vapor isotope standard source (Model 908-0003-9002; Los Gatos Research). The calibration was performed every 3 h. Each calibration cycle consisted of 5 concentrations and lasted for 30 min in total. Other details of this experiment can be found in Xiao et al. (2017).

Errors in the vapor isotope ratio measured by IRIS analyzers can arise from concentration dependence and from scale expansion or delta stretching, but with the former dominating the latter (Wen et al., 2008; Wen et al., 2012b). An ideal calibration strategy is to correct the measurement for both errors. However, cycling through vapor standards at multiple

concentration and multiple delta values would take too much instrument time away from ambient measurement. At Zhangye and Lake Taihu, the calibration method deployed only one isotopic standard but at multiple concentration values, which aimed at removing the concentration dependence. A comparison between calibration using one delta standard versus that using multiple delta standards indicates that the one-delta calibration may introduce an error of about 0.1‰ (Wen et al., 2012b).

2.2 Regression models

In this study, three regression models were used with the Keeling plot method to obtain the intercept of Eq. (1): ordinary least squares regression (OLS), geometric mean regression (GMR), and York's solution (YS). The OLS seeks to minimize the sum of the squared residuals between the expected values of the dependent variable y and the data points. The result is unbiased only if errors in the independent variable x are negligible and errors in y are constant. The GMR seeks to minimize both the vertical (dependent variable, y) and horizontal (independent, x) residuals. The result is unbiased only when the normalized error in x , or error in x divided by the variance of x , is equal to the normalized error in y (Kermack & Haldane, 1950). Generally, both x and y have measurement errors, and these errors may also be correlated. While neither the OLS nor the GMR method accounts for the error correlation, the YS method takes the correlation between errors in x and errors in y into account to obtain a best-fit straight line (York, 1966, 1969; York et al., 2004). Other details on the regression models can be found in Chen et al. (2017) and Wehr and Saleska (2017).

2.3 Characterization of error structures

The error parameters in the YS model, $\sigma(x_i)$, $\sigma(y_i)$ and r_i , for Lake Taihu were determined with the field calibration data. Here $\sigma(x_i)$ and $\sigma(y_i)$ are errors in horizontal ($1/c$) and vertical (δ_v) coordinates at the i th datapoint, and r_i is correlation between errors in x_i and errors in y_i . A calibration cycle consisted of 5 concentrations, each lasting for 6 min. An example of the calibration stepping is given by Xiao et al. (2017; their Figure 4). The standard deviation of $1/c$, the standard deviation of δ_v and the correlation coefficient between $1/c$ and δ_v were calculated for each concentration interval. We assumed that these variations originated purely from measurement errors. The data during transition from one concentration level to the next were excluded from the calculation.

For Zhangye, the field calibration data cannot be used to characterize the measurement errors because the concentration of the water vapor generated by the liquid vaporization module was not stable during the calibration phase. To obtain the error parameters, we carried out additional measurements using the same IRIS water vapor isotope analyzer deployed in the field. The analyzer was configured to measure the water vapor concentration and the isotopic composition of a water vapor stream generated by a standard delivery module (Model A0101; Picarro Inc.), a different calibration unit than what was deployed in the field. This delivery module was fed with liquid water of known δ_v value (-9.17‰). Each measurement cycle included 3 water vapor concentrations and lasted for 1 h. A total of 141 measurement cycles were performed, with the vapor concentration ranging from 7,900 ppm to 27,690 ppm. The same method used for Lake Taihu was used to calculate the error parameters.

2.4 Data processing

The high-frequency IRIS data were used to calculate δ_E for each hourly observation interval. In the flux-gradient method, the data were averaged to obtain the mean concentration differences between the two measurement heights, and δ_E was determined from the gradient ratio according to Eq. (2) after span correction as described by Lee et al. (2007).

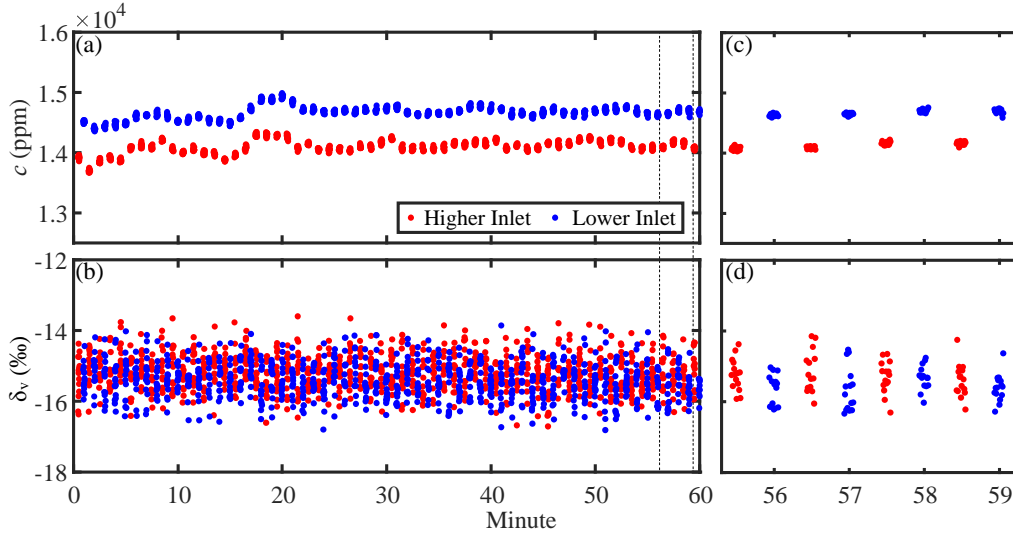


Figure 1. Temporal variation of H₂O mixing ratio (a) and δ_v (b) at the lower inlet (blue dots) and higher inlet (red dots) at Lake Taihu between 16:00 and 17:00 local time on October 22nd, 2014. Panels c and d are the corresponding zoom-in plot of the dotted box in panels a and b.

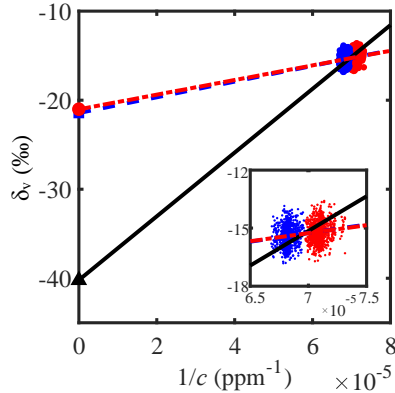


Figure 2. An illustration of the three regression models applied to the data in Figure 1. YS: red-dot-dashed line, $\delta_E = -21.02\text{‰}$; OLS: blue-dashed line, $\delta_E = -21.43\text{‰}$; GMR: black-solid line, $\delta_E = -40.21\text{‰}$; blue dots: observations at lower inlets; red dots: observations at higher inlet. In this hour, the δ_E obtained from the flux-gradient method is -21.00‰ , with a standard deviation of 4.78‰ .

In the Keeling plot method, the three regression models described above were used to determine δ_E . Each observation, including data obtained for both measurement heights, consisted of about 200 and 1,800 data points for Zhangye and Lake Taihu, respectively. Figure 1 shows the time series of the water vapor mixing ratio and the calibrated vapor δ_v from a typical observation period at Lake Taihu, and Figure 2 shows the corresponding linear regression plot.

Three criteria were used to screen the data. The flux-gradient method becomes noisy at times of small vertical concentration gradients. To ensure a robust comparison, we restricted our analysis to observations whose hourly mean vertical vapor concentration difference between the two measurement heights was larger than 200 ppm in magnitude. About 2/3 of the 3,026 and 1,622 valid observations satisfy this criterion at Zhangye and Lake Taihu, respectively. The second criterion was the standard deviation of δ_E calculated by the flux-gradient method; we used a threshold value of 20%. The third criterion required that the P value obtained from the Keeling plot method be smaller than 0.05 to ensure that the relationship between $1/c$ and δ_v passes the significance test (Unger et al., 2010). A total of 1,084 and 817 hourly observations remained for Zhangye and Lake Taihu, respectively, after the three data screening criteria were applied.

2.5 Craig-Gordon model of lake δ_E

The Craig-Gordon model was used to evaluate the bias errors of the Keeling plot and the flux-gradient methods for the lake site. The model computes δ_E as,

$$\delta_E = \frac{\alpha_{eq}^{-1} \delta_L - h \delta_v - \varepsilon_{eq} - (1-h) \varepsilon_k}{1 - h + 0.001(1-h) \varepsilon_k} \quad (3)$$

where α_{eq} (> 1) is the equilibrium fractionation factor which is a known function of water surface temperature (Majoube, 1971), δ_L is the isotopic composition of the lake surface water, h

is relative humidity in fraction, $\varepsilon_{\text{eq}} = 10^3(1 - 1 / \alpha_{\text{eq}})$ is the equilibrium factor in delta notation (‰), and ε_k is isotopic kinetic fractionation factor (‰). The calculation was performed at hourly intervals using the measured variables as inputs. The kinetic factor was calculated with the wind-dependent parameterization of Merlivate and Jouzel (1979). This parameterization was independently validated against the measured local evaporation line and the isotopic mass balance of the lake (Xiao et al., 2017).

3 Results and Discussion

3.1 YS model with two different error structures

The relationships between the water vapor concentration and the standard deviation of $1/c$, the standard deviation of δ_v and correlation coefficient r , established with the data collected during the instrument calibration cycles, are shown in Figure 3. Unsurprisingly, the standard deviation of $1/c$ was greater at lower concentrations, with the Picarro analyzer (used at Zhangye) and the LGR analyzer (used at Lake Taihu) giving similar performance. The standard deviation of $1/c$ was 4.02×10^{-7} and $4.07 \times 10^{-7} \text{ ppm}^{-1}$ at a water vapor concentration of 10,000 ppm and 1.29×10^{-7} and $7.26 \times 10^{-8} \text{ ppm}^{-1}$ at a concentration of about 30,000 ppm, for Zhangye and Lake Taihu, respectively. The standard deviation of δ_v showed opposite trends for the two sites. At Zhangye, the standard deviation of δ_v was relatively constant at concentrations lower than about 20,000 ppm and increased slightly with increasing concentration beyond this threshold. At Lake Taihu, the standard deviation of δ_v showed a general decreasing trend with increasing concentration. At Zhangye, the correlation between measurement errors in $1/c$ and in δ_v was slightly positive at low concentrations ($\sim 10,000$ ppm) and varied around zero at high

concentrations ($\sim 25,000$ ppm). At Lake Taihu, the error correlation was mostly positive and did not seem to depend on the vapor concentration.

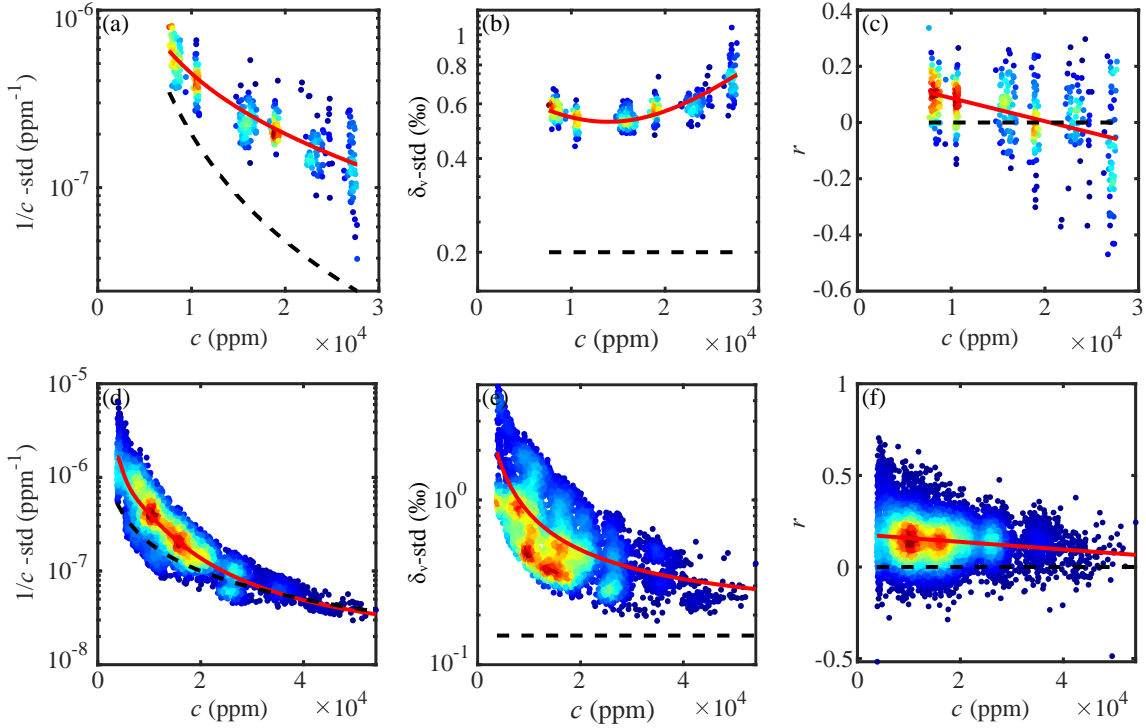


Figure 3. Relationships between water vapor concentration and errors in $1/c$, errors in δ_v and correlation coefficient between errors in δ_v and errors in $1/c$ for Zhangye (a, b and c) and Lake Taihu (d, e and f). The solid red line and black dash line indicate the regression fit and the precision given by the manufacturers, respectively. The regression equations are given in Supplementary Table S1. Color indicates data density.

For comparison, Figure 3 also shows error structures based on manufacturers' specifications. Specifically, the 0.1 Hz error (precision) is 20 ppm for water vapor and 0.20‰ for $\delta^{18}\text{O}$ for Zhangye and the 1 Hz error is $0.002c$ for water vapor and 0.15‰ for $\delta^{18}\text{O}$ for Lake Taihu, and the correlation between the two variables is set to zero as in Wehr and Saleska (2017). Generally, field errors were much larger than those specified by the manufacturers except for $1/c$ at the high concentration range at Lake Taihu where the two were similar.

Results of regression fitting (Table S1) to the data shown in Figure 3 were used to determine parameters $\sigma(x_i)$, $\sigma(y_i)$ and r_i in the YS regression model as functions of the measured concentration at time i , c_i . For example, the error in the vertical axis (δ_v) at time i is given as $\sigma(y_i) = f_y(c_i)$, where f_y is the regression fitting equation on c_i .

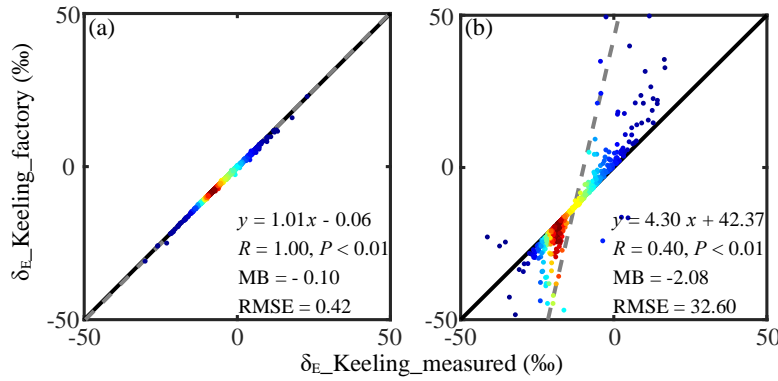


Figure 4. Comparison of the YS regression results with factory error structure and with measured error structure for Zhangye (a) and Lake Taihu (b). Solid black lines are the 1:1 comparison and gray dash line is linear regression. The regression equation is shown in each panel along with the correlation coefficient R , mean bias (MB, ‰) and root mean squares error (RMSE, ‰). In panel b, 19 datapoints are out of the range of the vertical axis ($\pm 50\%$). Color indicates data density.

Figure 4 compares the YS calculation using the factory and measured error structures. Nearly identical results were obtained for Zhangye using the two different error structures. (panel a, linear correlation $R = 1.00$, $RMSE = 0.42\%$). This contrasts sharply with Lake Taihu, where the YS model with the manufacturer's error specification performed poorly against the YS estimate with field errors ($R = 0.40$, $RMSE = 32.60\%$, Figure 4b), or against the OLS model ($R = 0.42$, $RMSE = 32.44\%$), the flux-gradient method ($R = 0.33$, $RMSE = 33.15\%$), and the Craig-Gordon model ($R = 0.32$, $RMSE = 34.29\%$; Figure S1). At the lake site, use of the field error structures significantly improved the YS estimate in comparison with the OLS regression model ($R = 0.99$, $RMSE = 1.45\%$), the flux gradient method ($R = 0.84$, $RMSE = 4.60\%$) and the Craig-

Gordon calculation ($R = 0.65$, $RMSE = 6.93\%$; Table 2). The disparity between the two YS estimates resulted from the fact the reported manufacturer's error for δ_v is too small and is concentration-independent, but the actual error was higher and was also very sensitive to concentration (Figure 3; Salmon et al., 2019; Sturm & Knohl, 2010). The problem is particularly severe at the low concentration range, where according to the manufacturer, the normalized error in $1/c$ is 0.013 and is only marginally better than the normalized error in δ_v (0.020; Table 3). When normalized errors in the dependent and independent variables are comparable, the YS model behaves like the GMR model (Wehr and Saleska, 2017).

In the following, we will restrict our discussion to the YS results using the measured error structures.

Table 1. Comparison between the flux-gradient (FG) method and the Keeling plot method with YS, OLS and GMR regression models for Zhangye, showing the linear regression, correlation coefficient (R), mean bias (MB, %) and root mean squares error (RMSE, %). The mean bias is calculated as the estimate using the method in the column header minus that using the method listed in the row header.

		FG	Keeling with YS	Keeling with OLS
Keeling with YS	Equation	$y = 0.95x + 0.59$		
	R	0.70		
	MB	0.93	—	—
	RMSE	4.48		
Keeling with OLS	Equation	$y = 0.92x + 0.17$	$y = 0.97x - 0.41$	
	R	0.70	1.00	
	MB	0.73	-0.20	—
	RMSE	4.39	0.48	
Keeling with GMR	Equation	$y = 1.73x + 12.47$	$y = 1.82x - 11.40$	$y = 1.88x + 12.16$
	R	0.52	0.72	0.69
	MB	7.48	6.75	6.75
	RMSE	11.40	9.68	10.01

Table 2. Comparison among the flux-gradient (FG) method, the Craig-Gordon model calculation (CG) and the Keeling plot method with YS, OLS and GMR regression models for Lake Taihu, showing the linear regression, correlation coefficient (R), mean bias (MB, ‰) and root mean squares error (RMSE, ‰). The mean bias is calculated as the estimate using the method in the column header minus that using the method listed in the row header.

		CG	FG	Keeling with YS	Keeling with OLS
FG	Equation	$y = 0.99x + 0.18$			
	R	0.72			
	MB	0.31	—	—	—
	RMSE	5.96			
Keeling with YS	Equation	$y = 1.02x + 1.86$	$y = 1.00x + 1.07$		
	R	0.65	0.84		
	MB	1.50	1.01	—	—
	RMSE	6.93	4.60		
Keeling with OLS	Equation	$y = 0.96x - 0.10$	$y = 0.96x - 0.45$	$y = 0.96x - 1.47$	
	R	0.66	0.83	0.99	
	MB	0.48	0.14	-0.87	—
	RMSE	6.51	4.59	1.45	
Keeling with GMR	Equation	$y = 4.18x + 46.02$	$y = 4.21x + 45.24$	$y = 4.19x + 40.73$	$y = 4.39x + 47.20$
	R	0.53	0.68	0.79	0.80
	MB	-0.91	-1.66	-2.67	-1.80
	RMSE	30.18	28.64	27.64	27.72

3.2 Comparison between the flux-gradient and the Keeling plot methods

3.2.1 Comparison statistics

A comparison between the flux-gradient method and the Keeling plot method using the three regression models is summarized in Tables 1 and 2. Figure 5 shows the comparison in 1:1 plots, where each data point represents one hourly δ_E calculated using data from two measurement heights above the surface. The Keeling plot results with the YS and OLS regression models and the flux-gradient results were comparable, with the relative mean biases less than 1.01‰ among each other and high linear correlations ($R > 0.70$) for both Zhangye and Lake Taihu.

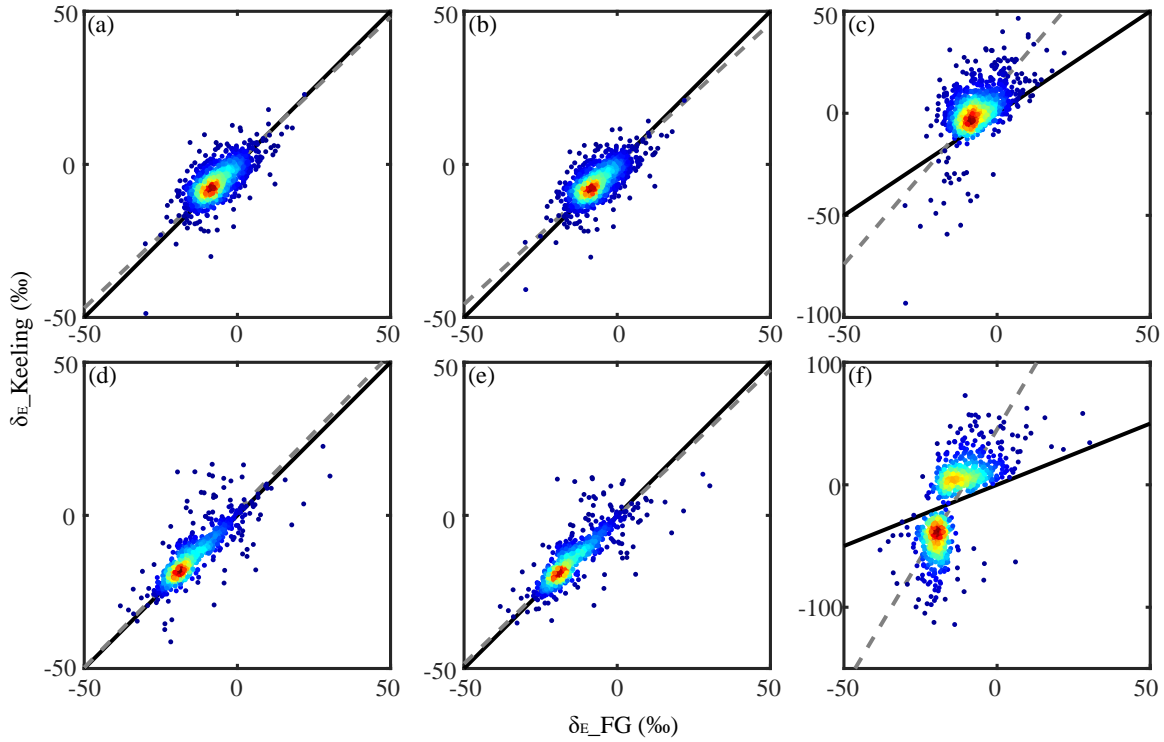


Figure 5. Comparison of the evaporation isotopic signature δ_E obtained with the flux-gradient method and with the Keeling plot method for Zhangye (a, b and c) and Lake Taihu (d, e and f). Panels a and d: YS regression model; panels b and e: OLS regression model; panels c and f: GMR regression model. Solid lines are the 1:1 comparison and dashed lines are linear regression. Refer to Tables 1 and 2 for regression statistics. Color indicates data density.

In contrast, the GMR results were rather poor in comparison with the OLS, the YS or the flux-gradient method results. For example, the mean bias against the flux-gradient method was large, at 6.97 and -1.66‰ for Zhangye and Lake Taihu, respectively. An implicit assumption of GMR is that the normalized errors in x and y are equal (Kermack & Haldane, 1950). This assumption was not satisfied here. Table 3 shows the mean errors in $1/c$ and δ_v , and these errors normalized by the ranges of $1/c$ and δ_v for three levels of water vapor concentration. Here the range of a variable is defined as the difference between the maximum and the minimum value of the high-frequency data in a given 60-min observational period. Errors existed both in the horizontal coordinate, $1/c$, and the vertical coordinate, δ_v . The normalized error in δ_v was,

however, much larger than the normalized error in $1/c$, by a factor of 6 to 10 at Zhangye and of 4 to 6 at Lake Taihu.

Some researchers advocate for the Miller-Tans equation (Miller & Tans, 2003) instead of the Keeling plot equation (Eq. (1)) when using the GMR model,

$$c\delta_v = \delta_E c + a \quad (4)$$

In Eq. (4), the slope parameter is equivalent to the isotopic composition of surface evaporation. We used the OLS and the GMR models to estimate the slope parameter in Eq. (4) and compared the results with the Keeling plot method using the OLS model (Figure S2). The Miller-Tans slope from OLS was nearly identical to the Keeling plot intercept from OLS. However, the Miller-Tans slope from GMR showed large deviations from the Keeling plot intercept from OLS. Comparison of the Miller-Tans method using GMR with estimates from Keeling plot method with YS, the flux-gradient method or the Craig-Gordon calculation yielded similarly large deviations. It appears that the GMR was not a good regression model for the high-frequency water vapor data deployed in this study, regardless of whether the Keeling plot equation or the Miller-Tans equation was used.

Table 3. Measurement errors in three quantiles of water vapor concentration. Errors are calculated as one standard deviation of high frequency data (0.2 Hz at Zhangye and 2 Hz at Lake Taihu). Here c and δ_v denote water vapor concentration and vapor δ_v , respectively. Numbers in parentheses are using error estimates from instrument manufacturers.

Quantile	Mean c ppm	Error in $1/c$ ppm^{-1}	Error in δ_v ‰	c range ppm	δ_v range ‰	$1/c$ range ppm^{-1}	Error in $1/c$ / ($1/c$ range)	Error in δ_v / (δ_v range)
Zhangye								
0 - 25	7688	5.86×10^{-7} (3.38×10^{-7})	0.57 (0.20)	1856	3.48	3.64×10^{-5}	0.016 (0.009)	0.16 (0.057)
25 - 75	12984	3.32×10^{-7} (1.19×10^{-7})	0.53 (0.20)	2659	3.50	1.65×10^{-5}	0.020 (0.007)	0.15 (0.057)
75 - 100	18930	2.16×10^{-7} (5.58×10^{-8})	0.55 (0.20)	3566	3.95	1.02×10^{-5}	0.021 (0.005)	0.14 (0.051)
Lake Taihu								
0 - 25	9171	4.58×10^{-7} (2.18×10^{-7})	0.88 (0.15)	1262	7.43	1.73×10^{-5}	0.026 (0.013)	0.12 (0.020)
25 - 75	21213	1.25×10^{-7} (9.43×10^{-8})	0.49 (0.15)	1697	3.29	4.27×10^{-6}	0.029 (0.022)	0.15 (0.046)
75 - 100	30879	6.96×10^{-8} (6.48×10^{-8})	0.40 (0.15)	2232	3.11	2.35×10^{-6}	0.030 (0.028)	0.13 (0.064)

The above results differ from the conclusions reported for carbon isotopes of CO₂ in two respects. First, Pataki et al. (2003) reported that the GMR intercept is systematically more negative than the OLS intercept when applied to the calculation of the ¹³C composition of ecosystem respiration. In our study, the δ_E from the GMR could be biased either high or low in reference to OLS. At Zhangye, almost all the datapoints were located above the 1:1 line (Figure 5c), indicating that GMR was biased positively compared to OLS. At Lake Taihu, the bias was mostly positive when the δ_E from the Keeling plot method with the GMR was greater than -15‰ and mostly negative when δ_E was less than -15‰. Second, increasing CO₂ concentration range will reduce the systematic bias associated with the $\delta^{13}\text{C}$ signature of respired CO₂ inferred from the Keeling plot method with the OLS model. This is true for observations made with flasks (Pataki et al., 2003; Zobitz et al., 2006) and IRIS instruments (Chen et al., 2017; Zobitz et al., 2006) and for synthetic CO₂ datasets (Kaylor et al., 2010; Wher & Saleska, 2017). In the case of water vapor, the performance of the OLS model, in reference to the flux-gradient method or the YS estimate, did not show obvious dependence on concentration range (Figure S3 and S4).

3.2.2 Results from Keeling plot method with single-height data

Logistically, it is much easier to measure the water vapor isotopic composition at a single height than at multiple heights involving valve switching. Indeed, the great majority of the published IRIS water vapor isotope measurements have been conducted with single-height configurations (Fiorella et al., 2018; Wei et al., 2019; Yao et al., 2018; Zannoni et al., 2019a). Here, we applied the Keeling plot method to data collected at the lower measurement height and compared the results with the flux-gradient method (Figure S5). All the three regression models performed less well when only data from the lower height was used than when data from both heights were used

to perform the regression (Figure 5). For example, at Lake Taihu, the mean difference of the OLS against the flux-gradient method changed to 0.44‰ (Figure S5e) from 0.14‰ (Figure 5e) and the correlation between the Keeling plot method and the flux-gradient method was reduced to 0.33 from 0.83.

The deteriorated performance in Figure S5 resulted in part from a reduced sample size and from a narrower concentration range which increase the uncertainty of the Keeling plot results (Chen et al., 2017; Pataki et., 2003; Zobitz et al., 2006). The sample size was halved when only one-height measurement was used. The mean concentration ranges were 2,063 and 1,137 ppm for Zhangye and Lake Taihu, respectively, for the data shown in Figure S5, whereas the mean ranges were larger, at 2,534 and 1,712 ppm for Zhangye and Lake Taihu, respectively, in Figure 5. Similarly, Good et al. (2012) reported that the uncertainty of the isotopic composition of evapotranspiration associated with high-frequency time series measured at a single height is 25% larger than with a combined use of time series measured at multiple heights.

While the systematic biases of the GMR regression in Figure S5 (panels c and f) are mathematical in nature (as in Figure 5 panels c and f), the biases of the OLS and the YS regression here may be related to footprint influences, especially at Zhangye where the fetch was short (about 200 m). Griffis et al. (2007) found that the Keeling plot method with one-height data yields lower estimates of the $\delta^{13}\text{C}$ composition of ecosystem respiration of a C_4 crop than the flux-gradient method. They attributed this difference to a footprint mismatch: the single-height concentration has a much larger source area and is therefore more influenced by the surrounding C_3 crops, than the flux-gradient data. Interestingly, Good et al. (2012) also found higher δ_{E} values

with the Keeling plot method using single-height data than using data from multiple heights (mean difference about 16‰ for ^{18}O , black triangles in their Figure 8).

3.3 Comparison with the Craig-Gordon model

It is believed that the Craig-Gordon model accurately predicts the δ_E of evaporating water bodies, and we tested the δ_E determined with the flux-gradient method and the Keeling plot method using each of the three regression models at Lake Taihu against this benchmark (Figure 6). The comparison statistics are summarized in Table 2. Once again, the GMR result showed a very large RMSE (30.18‰). The flux-gradient method and the Keeling plot method with the OLS and the YS regression were comparable in terms of linear correlation and RMSE. Of these three estimates, the flux-gradient and the OLS regression showed a small mean bias (MB) of 0.31‰ and 0.48‰, respectively, and the MB of the YS regression was larger, at 1.50‰.

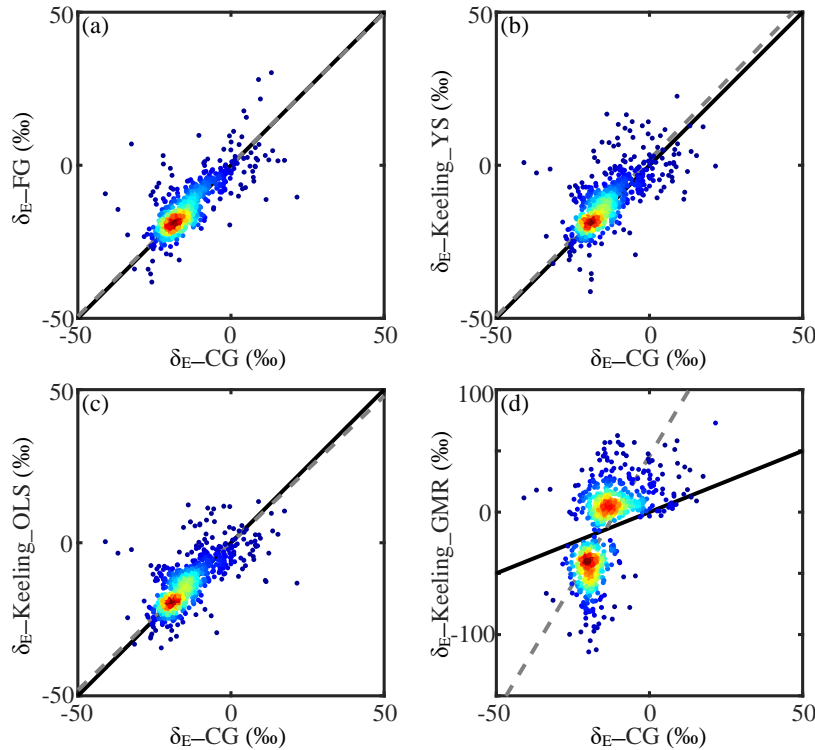


Figure 6. Comparison of the evaporation isotopic signature δ_E against the Craig-Gordon (CG) model calculation for Lake Taihu: flux-gradient method (a), and Keeling plot method with the

YS (b), the OLS (c) and the GMR (d) regression models. Solid lines are the 1:1 comparison and dashed lines are linear regression. Refer to Table 2 for regression statistics. Color indicates data density.

The relative larger bias between YS and Craig-Gordon begs the question of whether the Craig-Gordon model of isotopic evaporation can be used to benchmark the performance of the flux-gradient method or the Keeling plot method. For a given hourly period, measurement errors in the Craig-Gordon input variables can propagate through the model to cause errors in the calculated δ_E . This type of error should be random. One potential source of systematic Craig-Gordon error lies in the parameterization of the kinetic fractionation of evaporation. In the present study, we used the wind dependent parameterization of Merlivat and Jouzel (1979), which has been validated independently against the observed local evaporation line and the observed lake evaporation (Xiao et al., 2017). The mean kinetic factor for the observations shown in Figure 6 was 7.3‰. Forcing the Craig-Gordon model to remove the mean bias with the YS result would require that the mean kinetic factor be lowered to 5.8‰. Such a small kinetic factor seems unphysical because it is lower than other values used in the literature for inland water bodies (Gonfiantini et al., 2018; Jasechko et al., 2014) and is even lower than that for the open ocean (Merlivat and Jouzel, 1979). Instead, we suggest that the relative bias between YS and Craig-Gordon stemmed from the error structure used for YS. The instrument errors were highly sensitive to concentration. The error structure shown in Figure 3 was based on measurement taken during instrument calibration cycles. While it was much better than the error structure based on the instrument specification, it may still deviate from the true measurement errors.

4 Summary and Conclusions

The YS regression can be sensitive to how measurement errors are specified. For Lake Taihu, the YS regression yielded rather poor estimates of δ_E if it employed the error structures provided by the instrument manufacturer. Use of the error structures from field observations significantly improved the YS estimate in comparison with the OLS regression, the flux-gradient method and the Craig-Gordon model calculation. This difference resulted mainly from the fact that the manufacturer default error value for δ_v is invariant with the vapor concentration whereas the actual error was highly dependent on the concentration.

The Keeling plot results with the YS (using field error structures) and OLS regression and the flux-gradient results were comparable, with the mean difference in the hourly δ_E of less than 1.01‰ and with high linear correlation ($R = 0.70$ to 1.00) for both Zhangye and Lake Taihu. These results were obtained with high frequency measurements made at two heights above the surface. The agreement with the flux-gradient method deteriorated ($R = 0.29$ to 0.49) if one-height data was used to perform the YS and the OLS regression. In general, the GMR results were poor in comparison with the OLS and the YS regression or with the flux-gradient method. Unlike in studies of carbon isotopes, here the GMR bias in reference to the OLS regression could be either positive or negative. Use of the Miller-Tans instead of the Keeling plot equation did not bring improvement to the GMR performance.

At Lake Taihu, the flux-gradient method and the Keeling plot method with the OLS and the YS regression (using field error structures) were comparable to the Craig-Gordon model calculation in terms of linear correlation R (0.66 to 0.72) and RMSE (5.96 to 6.93%). The mean

bias error in δ_E was small for the flux-gradient method (0.31‰) and the Keeling plot method with the OLS regression (0.48‰), indicating that these methods were both robust, at least for this site with large fetch conditions. The mean bias of the YS regression was larger (1.50‰), suggesting room for further improvement of the error structures used for YS.

Our results favor the OLS over the YS regression when using the Keeling plot method for studies of isotopic evaporation. In principle, YS is the best choice of the three regression models (Wehr & Saleska, 2017). However, implementation of the YS regression requires that measurement errors in the concentration and in the isotopic composition be known accurately. Wehr and Saleska (2017) found that the YS regression with factory-specified errors yields the least biased result for CO₂ isotopes. In the present study, the YS regression with factory-specified errors worked well for one instrument (Picarro at Zhangye) but not for the other (LGR at Lake Taihu). Our results favor the OLS over the YS regression because it is a simpler calculation and especially when measurement errors in field conditions are unavailable.

Acknowledgements

The authors would like to thank all the participants of the experiments at Zhangye and at Taihu Eddy Flux Network. They are grateful to the two journal reviewers whose constructive comments have significantly improved the manuscript. This work was supported by the National Key R&D Program of China (grant 2019YFA0607202), China Scholarship Council, the National Natural Science Foundation of China (grant 41975143) and the U.S. National Science Foundation (grant 1520684). The water vapor isotope data used in this study are available on the website <https://vapor-isotope.yale.edu>.

References

- Bowen, G. J., Cai, Z., Fiorella, R. P., & Putman, A. L. (2019). Isotopes in the water cycle: Regional- to global-scale patterns and applications. *Annual Review of Earth and Planetary Sciences*, 47, 457–479. <https://doi.org/10.1146/annurev-earth-053018>
- Bowling, D. R., Baldocchi, D. D., & Monson, R. K. (1999). Dynamics of isotopic exchange of carbon dioxide in a tennessee deciduous forest. *Global Biogeochemical Cycles*, 13(4), 903–922. <https://doi.org/10.1029/1999GB900072>
- Bowling, D. R., Burns, S. P., Conway, T. J., Monson, R. K., & White, J. W. C. (2005). Extensive observations of CO₂ carbon isotope content in and above a high-elevation subalpine forest. *Global Biogeochemical Cycles*, 19(3). <https://doi.org/10.1029/2004GB002394>
- Chen, C., Pang, J., Wei, J., Wen, X., & Sun, X. (2017). Inter-comparison of three models for $\delta^{13}\text{C}$ of respiration with four regression approaches. *Agricultural and Forest Meteorology*, 247, 229–239. <https://doi.org/10.1016/j.agrformet.2017.08.002>
- Craig, H., & Gordon, L. I. (1965). Deuterium and oxygen 18 variations in the ocean and the marine atmosphere. In E. Tongiorgi (Ed.), *Stable isotopes in oceanographic studies and paleotemperatures* (pp. 9–130). Pisa: Consiglio Nazionale Delle Ricerche Laboratorio di Geologia Nucleare.
- Delattre, H., Vallet-Coulomb, C., & Sonzogni, C. (2015). Deuterium excess in the atmospheric water vapour of a Mediterranean coastal wetland: regional vs. local signatures. *Atmospheric Chemistry and Physics*, 15, 10167–10181. <https://doi.org/10.5194/acp-15-10167-2015>
- Dubbert, M., & Werner, C. (2019). Water fluxes mediated by vegetation: emerging isotopic insights at the soil and atmosphere interfaces. *New Phytologist*, 221(4), 1754–1763.

<https://doi.org/10.1111/nph.15547>

Fiorella, R. P., Poulsen, C. J., & Matheny, A. M. (2018). Seasonal patterns of water cycling in a deep, continental mountain valley inferred from stable water vapor isotopes. *Journal of Geophysical Research: Atmospheres*, 123, 7271–7291.

<https://doi.org/10.1029/2017JD028093>

Gat, J. R., Bowser, C. J., & Kendall, C. (1994). The contribution of evaporation from the Great Lakes to the continental atmosphere: estimate based on stable isotope data. *Geophysical Research Letters*, 21(7), 557–560. <https://doi.org/10.1029/94GL00069>

Gibson, J. J., Edwards, T. W. D., Bursey, G. G., & Prowse, T. D. (1993). Estimating evaporation using stable isotopes. *Nordic Hydrology*, 24, 79–94.

Gonfiantini, R., Wassenaar, L. I., Araguas-Araguas, L., & Aggarwal, P. K. (2018). A unified Craig-Gordon isotope model of stable hydrogen and oxygen isotope fractionation during fresh or saltwater evaporation. *Geochimica et Cosmochimica Acta*, 235: 224–236.

<https://doi.org/10.1016/j.gca.2018.05.020>

Good, S. P., Soderberg, K., Wang, L., & Caylor, K. K. (2012). Uncertainties in the assessment of the isotopic composition of surface fluxes: A direct comparison of techniques using laser-based water vapor isotope analyzers. *Journal of Geophysical Research: Atmospheres*,

117(D15). <https://doi.org/10.1029/2011JD017168>

Good, S. P., Soderberg, K., Guan, K., King, E. G., Scanlon, T. M., Caylor, K. K., et al. (2014). Seeking genericity in the selection of parameter sets: Impact on hydrological model efficiency. *Water Resources Research*, 50, 1410–1432.

<https://doi.org/10.1002/2013WR014333>

Good, S. P., Noone, D., & Bowen, G. (2015). Hydrologic connectivity constrains partitioning of

global terrestrial water fluxes. *Science*, 349(6244), 175–177.

<https://doi.org/10.1126/science.aaa5931>

Griffis, T. J., Baker, J. M., Sargent, S. D., Tanner, B. D., & Zhang, J. (2004). Measuring field-scale isotopic CO₂ fluxes with tunable diode laser absorption spectroscopy and micrometeorological techniques. *Agricultural and Forest Meteorology*, 124(1–2), 15–29.

<https://doi.org/10.1016/j.agrformet.2004.01.009>

Griffis, T. J., Lee, X., Baker, J. M., Sargent, S. D., King, J. Y. (2005). Feasibility of quantifying ecosystem–atmosphere C¹⁸O¹⁶O exchange using laser spectroscopy and the flux-gradient method, *Agricultural and Forest Meteorology*, 135, 44–60,

<https://doi.org/10.1016/j.agrformet.2005.10.002>

Griffis, T. J., Zhang, J., Baker, J. M., Kljun, N., & Billmark, K. (2007). Determining carbon isotope signatures from micrometeorological measurements: Implications for studying biosphere-atmosphere exchange processes. *Boundary-Layer Meteorology*, 123(2), 295–316.

<https://doi.org/10.1007/s10546-006-9143-8>

Griffis, T. J., Wood, J. D., Baker, J. M., Lee, X., Xiao, K., Chen, Z., et al. (2016). Investigating the source, transport, and isotope composition of water vapor in the planetary boundary layer. *Atmospheric Chemistry and Physics*, 16(8), 5139–5157. [https://doi.org/10.5194/acp-](https://doi.org/10.5194/acp-16-5139-2016)

[16-5139-2016](https://doi.org/10.5194/acp-16-5139-2016)

Horst, T. W. (1999). The footprint for estimation of atmosphere-surface exchange fluxes by profile techniques. *Boundary-Layer Meteorology*, 90(2): 171–188.

<https://doi.org/10.1023/A:1001774726067>

Huang, L., & Wen, X. (2014). Temporal variations of atmospheric water vapor δD and δ¹⁸O above an arid artificial oasis cropland in the Heihe River Basin. *Journal of Geophysical*

- Research: Atmospheres*, 119, 11456–11476. <https://doi.org/10.1002/2014JD021891>
- Jasechko, S., Gibson, J. J., & Edwards, T. W. D. (2014). Stable isotope mass balance of the Laurentian Great Lakes. *Journal of Great Lakes Research*, 40(2): 336–346. <https://doi.org/10.1016/j.jglr.2014.02.020>
- Kayler, Z. E., Ganio, L., Hauck, M., Pypker, T. G., Sulzman, E. W., Mix, A. C., & Bond, B. J. (2010). Bias and uncertainty of $\delta^{13}\text{CO}_2$ isotopic mixing models. *Oecologia*, 163(1), 227–234. <https://doi.org/10.1007/s00442-009-1531-6>
- Keeling, D. C. (1958). The concentration and isotopic abundances of atmospheric carbon dioxide in rural areas. *Geochimica et Cosmochimica Acta*, 13(4), 322–334.
- Kermack, A. K. A., & Haldane, J. B. S. (1950). Organic correlation and allometry. *Biometrika*, 37(1), 30–41.
- Lee, X., Smith, R., & Williams, J. (2006). Water vapour $^{18}\text{O}/^{16}\text{O}$ isotope ratio in surface air in New England, USA. *Tellus B: Chemical and Physical Meteorology*, 58(4): 293–304. <https://doi.org/10.1111/j.1600-0889.2006.00191.x>
- Lee, X., Kim, K., & Smith, R. (2007). Temporal variations of the $^{18}\text{O}/^{16}\text{O}$ signal of the whole-canopy transpiration in a temperate forest. *Global Biogeochemical Cycles*, 21(3). <https://doi.org/10.1029/2006GB002871>
- Lee, X., Huang, J., & Patton, E. G. (2012). A large-eddy simulation study of water vapour and carbon dioxide isotopes in the atmospheric boundary layer. *Boundary-Layer Meteorology*, 145(1), 229–248. <https://doi.org/10.1007/s10546-011-9631-3>
- Lee, X., Liu, S., Xiao, W., Wang, W., Gao, Z., Cao, C., et al. (2014). The Taihu Eddy Flux Network: An observational program on energy, water, and greenhouse gas fluxes of a large freshwater lake. *Bulletin of the American Meteorological Society*, 95(10), 1583–1594.

<https://doi.org/10.1175/BAMS-D-13-00136.1>

Lu, X., Liang, L. L., Wang, L., Jenerette, G. D., McCabe, M. F., & Grantz, D. A. (2017).

Partitioning of evapotranspiration using a stable isotope technique in an arid and high temperature agricultural production system. *Agricultural Water Management*, 179, 103–109. <https://doi.org/10.1016/j.agwat.2016.08.012>

Majoube, M. (1971). Fractionnement en oxygene 18 et en deuterium entre l'eau et sa vapeur.

Journal de Chimie Physique, 68(7–8), 1423–1436. <https://doi.org/10.1051/jcp/1971681423>

Merlivat, L., & Jouzel, J. (1979). Global climatic interpretation of the deuterium-oxygen 18 relationship for precipitation. *Journal of Geophysical Research*, 84(C8), 5029–5033.

<https://doi.org/10.1029/JC084iC08p05029>

Miller, J. B., & Tans, P. P. (2003). Calculating isotopic fractionation from atmospheric

measurements at various scales. *Tellus, Series B: Chemical and Physical Meteorology*, 55(2), 207–214. <https://doi.org/10.1034/j.1600-0889.2003.00020.x>

Ogée, J., Peylin, P., Ciais, P., Bariac, T., Brunet, Y., Berbigier, P., et al. (2003). Partitioning net ecosystem carbon exchange into net assimilation and respiration using $^{13}\text{CO}_2$

measurements: A cost-effective sampling strategy. *Global Biogeochemical Cycles*, 17(2). <https://doi.org/10.1029/2002gb001995>

Pataki, D. E., Ehleringer, J. R., Flanagan, L. B., Yakir, D., Bowling, D. R., Still, C. J., et al.

(2003). The application and interpretation of Keeling plots in terrestrial carbon cycle research. *Global Biogeochemical Cycles*, 17(1). <https://doi.org/10.1029/2001GB001850>

Quade, M., Klosterhalfen, A., Graf, A., Brüggemann, N., Hermes, N., Vereecken, H., &

Rothfuss, Y. (2019). In-situ monitoring of soil water isotopic composition for partitioning of evapotranspiration during one growing season of sugar beet (*Beta vulgaris*). *Agricultural*

- and *Forest Meteorology*, 266–267, 53–64. <https://doi.org/10.1016/j.agrformet.2018.12.002>
- Salmon, O. E., Welp, L. R., Baldwin, M. E., Hajny, K. D. Strirm, B. H., & Shepson, P. B. (2019). Vertical profile observations of water vapor deuterium excess in the lower troposphere. *Atmospheric Chemistry and Physics*, 19(17): 11525–11543. <https://doi.org/10.5194/acp-19-11525-2019>
- Simonin, K. A., Link, P., Rempe, D., Miller, S., Oshun, J., Bode, C., et al. (2014). Vegetation induced changes in the stable isotope composition of near surface humidity. *Ecohydrology*, 7(3), 936–949. <https://doi.org/10.1002/eco.1420>
- Sturm, P., & Knohl, A. (2010). Water vapor $\delta^2\text{H}$ and $\delta^{18}\text{O}$ measurements using off-axis integrated cavity output spectroscopy. *Atmospheric measurement techniques discussions*, 2(4): 2055–2085. <https://doi.org/10.5194/amtd-2-2055-2009>
- Sun, X., Wilcox, B. P., & Zou, C. B. (2019). Evapotranspiration partitioning in dryland ecosystems: A global meta-analysis of in situ studies. *Journal of Hydrology*, 576, 123–136. <https://doi.org/10.1016/j.jhydrol.2019.06.022>
- Unger, S., Máguas, C., Pereira, J. S., Aires, L. M., David, T. S., & Werner, C. (2010). Disentangling drought-induced variation in ecosystem and soil respiration using stable carbon isotopes. *Oecologia*, 163(4), 1043–1057. <https://doi.org/10.1007/s00442-010-1576-6>
- Vardag, S. N., Hammer, S., & Levin, I. (2016). Evaluation of 4 years of continuous $\delta^{13}\text{C}(\text{CO}_2)$ data using a moving Keeling plot method. *Biogeosciences*, 13(14), 4237–4251. <https://doi.org/10.5194/bg-13-4237-2016>
- Wang, S., Zhang, M., Che, Y., Chen, F., & Qiang, F. (2016). Contribution of recycled moisture to precipitation in oases of arid central Asia: A stable isotope approach. *Water Resources Research*, 52, 3246–3257. <https://doi.org/10.1111/j.1752-1688.1969.tb04897.x>

- Wang, X., & Yakir, D (2000). Using stable isotopes of water in evapotranspiration studies. *Hydrological Processes*, 14(8): 1407–1421. [https://doi.org/10.1002/1099-1085\(20000615\)14:8<1407::AID-HYP992>3.0.CO;2-K](https://doi.org/10.1002/1099-1085(20000615)14:8<1407::AID-HYP992>3.0.CO;2-K)
- Wehr, R., & Saleska, S. R. (2017). The long-solved problem of the best-fit straight line: Application to isotopic mixing lines. *Biogeosciences*, 14(1), 17–29. <https://doi.org/10.5194/bg-14-17-2017>
- Wei, Z., Lee, X., Wen, X., & Xiao, W. (2018). Evapotranspiration partitioning for three agro-ecosystems with contrasting moisture conditions: A comparison of an isotope method and a two-source model calculation. *Agricultural and Forest Meteorology*, 252, 296–310. <https://doi.org/10.1016/j.agrformet.2018.01.019>
- Wei, Z., Lee, X., Aemisegger, F., Benetti, M., Berkelhammer, M., Casado, M., et al. (2019). A global database of water vapor isotopes measured with high temporal resolution infrared laser spectroscopy. *Scientific Data*, 6, 180302. <https://doi.org/10.1038/sdata.2018.302>
- Welp, L. R., Lee, X., Kim, K., Griffis, T. J., Billmark, K. A., & Baker, J. M. (2008). $\delta^{18}\text{O}$ of water vapour, evapotranspiration and the sites of leaf water evaporation in a soybean canopy. *Plant, Cell and Environment*, 31(9), 1214–1228. <https://doi.org/10.1111/j.1365-3040.2008.01826.x>
- Welp, L. R., Lee, X., Griffis, T. J., Wen, X. F., Xiao, W., Li, S., et al. (2012). A meta-analysis of water vapor deuterium-excess in the midlatitude atmospheric surface layer. *Global Biogeochemical Cycles*, 26(3). <https://doi.org/10.1029/2011GB004246>
- Wen, X., Sun, X., Zhang, S., Yu, G., Sargent, S. D., & Lee, X. (2008). Continuous measurement of water vapor D/H and $^{18}\text{O}/^{16}\text{O}$ isotope ratios in the atmosphere. *Journal of Hydrology*, 349(3–4), 489–500. <https://doi.org/10.1016/j.jhydrol.2007.11.021>

- Wen, X., Lee, X., Sun, X., Wang, J., Hu, Z., Li, S., & Yu, G. (2012a). Dew water isotopic ratios and their relationships to ecosystem water pools and fluxes in a cropland and a grassland in China. *Oecologia*, 168(2), 549–561. <https://doi.org/10.1007/s00442-011-2091-0>
- Wen, X., Lee, X., Sun, X., Wang, J., Tang, Y., Li, S., & Yu, G. (2012b). Intercomparison of four commercial analyzers for water vapor isotope measurement. *Journal of Atmospheric and Oceanic Technology*, 29(2), 235–247. <https://doi.org/10.1175/JTECH-D-10-05037.1>
- Wen, X., Yang, B., Sun, X., & Lee, X. (2016). Evapotranspiration partitioning through in-situ oxygen isotope measurements in an oasis cropland. *Agricultural and Forest Meteorology*, 230–231, 89–96. <https://doi.org/10.1016/j.agrformet.2015.12.003>
- Xiao, W., Lee, X., Hu, Y., Liu, S., Wang, W., Wen, X., et al. (2017). An experimental investigation of kinetic fractionation of open-water evaporation over a large lake. *Journal of Geophysical Research: Atmospheres*, 122(21), 11,651–11,663. <https://doi.org/10.1002/2017JD026774>
- Xiao, W., Qian, Y., Lee, X., Wang, W., Zhang, M., Wen, X., et al. (2018). Hydrologic implications of the isotopic kinetic fractionation of open-water evaporation. *Science China Earth Sciences*, 61(10), 1523–1532. <https://doi.org/10.1007/s11430-018-9246-9>
- Yao, T., Zhang, X., Guan, H., Zhou, H., Hua, M., & Wang, X. (2018). Climatic and environmental controls on stable isotopes in atmospheric water vapor near the surface observed in Changsha, China. *Atmospheric Environment*, 189, 252–263. <https://doi.org/10.1016/j.atmosenv.2018.07.008>
- Yakir, D., & da SL Sternberg, L. (2000). The use of stable isotopes to study ecosystem gas exchange. *Oecologia*, 123(3): 297–311. <https://doi.org/10.1007/s004420051016>
- Yakir, D., & Wang, X. (1996). Fluxes of CO₂ and water between terrestrial vegetation and the

atmosphere estimated from isotope measurements. *Nature*, 380(6574): 515–517.

<https://doi.org/10.1038/380515a0>

Yepez, E. A., Williams, D. G., Scott, R. L., & Lin, G. (2003). Partitioning overstory and understory evapotranspiration in a semiarid savanna woodland from the isotopic composition of water vapor. *Agricultural and Forest Meteorology*, 119(1–2), 53–68.

[https://doi.org/10.1016/S0168-1923\(03\)00116-3](https://doi.org/10.1016/S0168-1923(03)00116-3)

Yepez, E. A., Huxman, T. E., Ignace, D. D., English, N. B., Weltzin, J. F., Castellanos, A. E., & Williams, D. G. (2005). Dynamics of transpiration and evaporation following a moisture pulse in semiarid grassland: A chamber-based isotope method for partitioning flux components. *Agricultural and Forest Meteorology*, 132(3–4), 359–376.

<https://doi.org/10.1016/j.agrformet.2005.09.006>

York, D. (1966). Least-squares fitting of a straight line. *Canadian Journal of Physics*, 44, 1079–1086.

York, D. (1969). Least squares fitting of a straight line with correlated errors. *Earth and Planetary Science Letters*, 5, 320–324.

York, D., Evensen, N. M., Martínez, M. L., & De Basabe Delgado, J. (2004). Unified equations for the slope, intercept, and standard errors of the best straight line. *American Journal of Physics*, 72(3), 367–375.

<https://doi.org/10.1119/1.1632486>

Zannoni, D., Steen-Larsen, H. C., Stenni, B., Dreossi, G., & Rampazzo, G. (2019a). Synoptic to mesoscale processes affecting the water vapor isotopic daily cycle over a coastal lagoon.

Atmospheric Environment, 197, 118–130. <https://doi.org/10.1016/j.atmosenv.2018.10.032>

Zannoni, D., Steen-Larsen, H. C., Rampazzo, G., Dreossi, G., Stenni, B., & Bergamasco, A. (2019b). The atmospheric water cycle of a coastal lagoon: An isotope study of the

interactions between water vapor, precipitation and surface waters. *Journal of Hydrology*,
572, 630–644. <https://doi.org/10.1016/j.jhydrol.2019.03.033>

Zobitz, J. M., Keener, J. P., Schnyder, H., & Bowling, D. R. (2006). Sensitivity analysis and
quantification of uncertainty for isotopic mixing relationships in carbon cycle research.
Agricultural and Forest Meteorology, 136(1–2), 56–75.
<https://doi.org/10.1016/j.agrformet.2006.01.003>